Response document formatting: Reviewer comments are shown in **black**, while our responses and revisions are shown in **blue** for clarity.

Referee #1

This paper provides a detailed study using an inverse model to update the methane emission inventory for India based on satellite data from GOSAT, TROPOMI and GHGSat. The study seems very thorough, the paper is well written, and the results are clearly presented. Furthermore, they are relevant to policy making and provide an important advance for developing methane reduction strategies.

My one quibble is that GHGSat data are mentioned, but we never really see a map of the retrievals. It would be nice to see some of these above the cities with increased landfill emissions.

I am happy to recommend publication.

Author Response:

Thank you very much for your positive and encouraging assessment of our manuscript. We greatly appreciate your comments regarding the quality and relevance of the study. We have added GHGSat observations for each landfill in supplementary Figure S4 to Figure S20. As mentioned in their captions, these images show data made available by Dogniaux et al. (2025).

Referee #2

The authors apply IMI/GEOS-Chem (0.25°×0.3125°) with the blended TROPOMI+GOSAT product (Balasus et al., 2023) to estimate 2021 Indian methane emissions, supplemented with facility-level GHGSat landfill data, and report a national total of 34.4 (32.0 to 40.4) Tg yr^{-1} with a 30-member ensemble. The study is well written and makes real contributions, namely the high state-vector resolution relative to earlier national studies, the use of GHGSat facility data to improve landfill and wastewater separation, and the multi-scale policy framing. The national total is consistent with several independent estimates, which is reassuring for the aggregate. My concerns concentrate on the observation-error budget, the treatment of aerosol-related retrieval biases, the prior-dependence of the sectoral attribution, and the strength of validation. Also, several critical flaws exist in data preprocessing, observational error configuration, model validation and aerosol interference correction, which undermine the rationality and reliability of the research methodology. Because these concerns bear most directly on the sectoral conclusions, especially the -57% coal correction, rather than on the national total, and because they are addressable, I recommend major revision.

Author Response:

Thank you for your positive evaluation of our manuscript and for providing feedback to improve the paper. We have conducted additional analyses to address the reviewer’s concerns and provide detailed responses to each comment below.

Major comments

1. The observation-error budget is likely optimistic and is not justified for Indian conditions

The super-observation error variance is reported as (11.23 ppb)^2, built from = 15 ppb, = 0.55 and = 4.5 ppb, all transferred from a China inversion (Chen et al., 2023). There are two issues. First, these parameters were calibrated for a different domain, so the manuscript should demonstrate, rather than assume, their validity over India, where surface and aerosol conditions differ substantially. Second, an under-specified observation error inflates the effective weight of the observations in the cost function and therefore inflates the magnitude of the emission corrections, which are precisely the quantities (coal at -57% and oil and gas at +33%) that the paper reports as its headline findings. Given that residual surface-reflectance and aerosol artefacts in the TROPOMI XCH_4 product are documented to introduce errors well beyond the random retrieval noise (Lorente et al., 2021, 2023), and that the reliability of TROPOMI-based emission estimates has been shown to depend strongly on how the observational error budget is constructed (Zheng et al., 2026), I recommend an ensemble member with a markedly larger and, ideally, spatially and seasonally varying observation error, with the sectoral posteriors re-reported.

Author response:

The super-observation error calculation parameters $r_{retrieval}$ = 0.55 and $\sigma_{transport\,=}$ 4.5 ppb, were adopted from previous inversion studies over North America and the Middle East. The retrieval error, $\sigma_{retrieval}$ = 15 ppb, was estimated from the root-mean-square difference between the TROPOMI observations and prior simulations over our own study domain. Using these parameters, the error for each individual super-observation varies spatially, temporally, and seasonally with the number of observations that are averaged into a single super-observation (Figure S1; Equation 6). Therefore, the reported super-observation error variance of (11.23 ppb)^2 represents the mean value across all observations rather than a constant value assigned to every observation. The value ranges from (9.0 ppb)^2 to (15.0 ppb)^2. To make this clear, we have modified the sentence at Line 308 of the revised submission as:

"Our mean super-observation error variance is (11.23 ppb)^2 for the inversion domain, with values ranging from (9.0 ppb)^2 to (15.0 ppb)^2 depending on the number of observations averaged into a single super-observation. The spatial variation in the annual mean super observation error is shown in Figure S1b."

To evaluate the sensitivity of the inversion to $r_{retrieval,}$ $\sigma_{transport,}$ and $\sigma_{retrieval}$ we performed an additional residual-fitting analysis using eq (6) for the observations over India as shown in Figure R1. This yielded $r_{retrieval}$ = 0.59, $\sigma_{transport\,=}$ 4.4 ppb, and $\sigma_{retrieval}$ = 16.5 ppb, resulting in a mean super-observation error variance of (12.6 (10.4-16.4) ppb)^2, which is close to the originally used value. The corresponding posterior national methane emission is 34.4 Tg/yr (compared to 34.4 (32.0 – 40.4) Tg/yr in the base inversion), with individual state vector elements showing changes of 0.95 % to 1.2 % compared to the base inversion as shown in Figure R2. The sectoral posterior estimates also remained consistent and are clearly within the uncertainty ranges estimated using the ensemble, with coal mine emissions decreasing from 0.9 (prior) to 0.5 (posterior) Tg/yr, consistent in the base inversion estimate of 0.4 (0.3-0.6) Tg/yr (Figure R3).

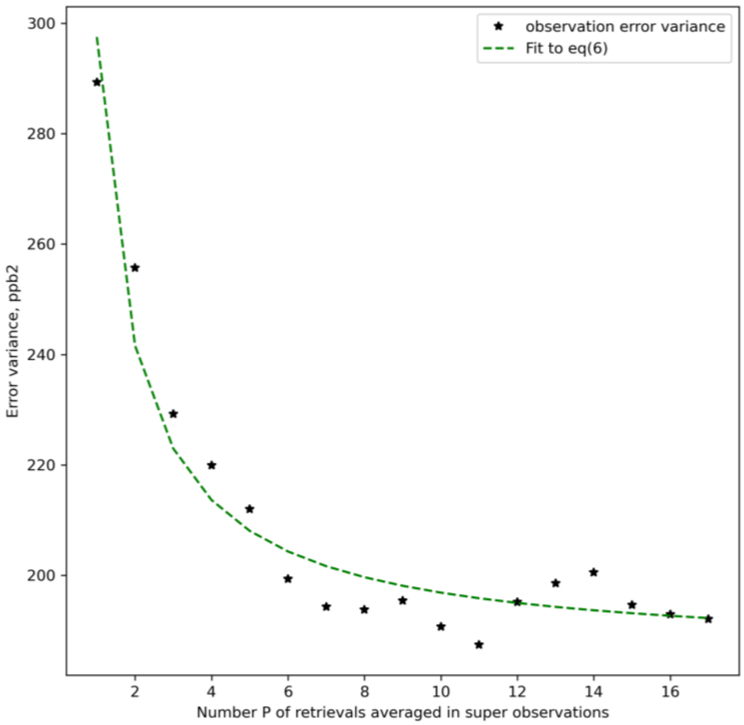

Figure R1. Reduction in super-observation error variance (σ^2_{super}) with increasing numbers of individual TROPOMI retrievals (P) averaged into each super-observation used in the inversion over the study domain. The star symbols represent the error variances estimated using the residual error method from the number of individual retrievals contributing to each super-observation. Each symbol summarizes the statistics from at least 100,000 super-observations. The solid line shows the two-component fit to the observational error variance described by Eq. (6).

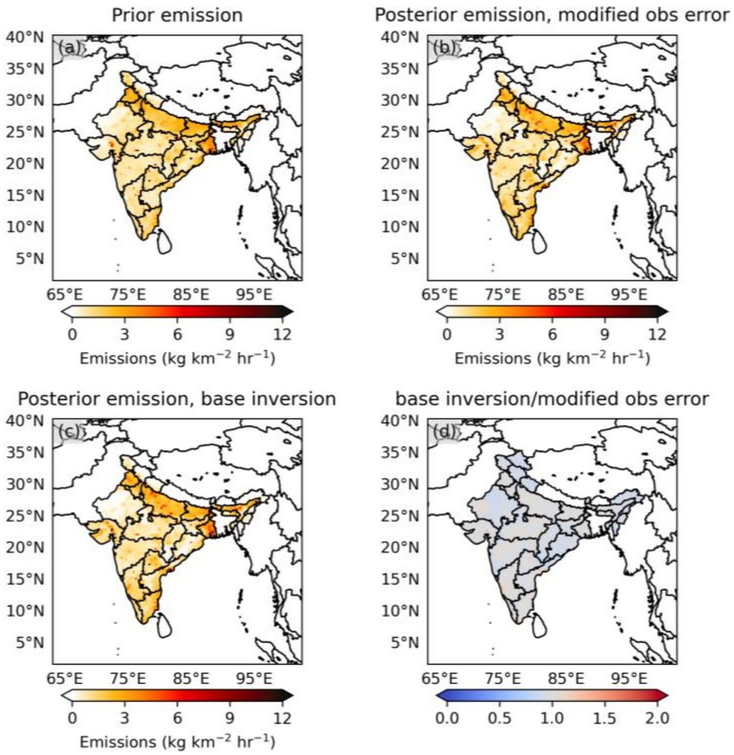

Figure R2. Prior (a), posterior (b) emissions derived using the modified super observational error, posterior emissions from the base inversion and the ratio of posterior emissions from the base and modified inversions (d) over India for 2021 (Borders are taken from Natural Earth (https://www.naturalearthdata.com/about/map-update-committee/), which provides de facto administrative boundaries).

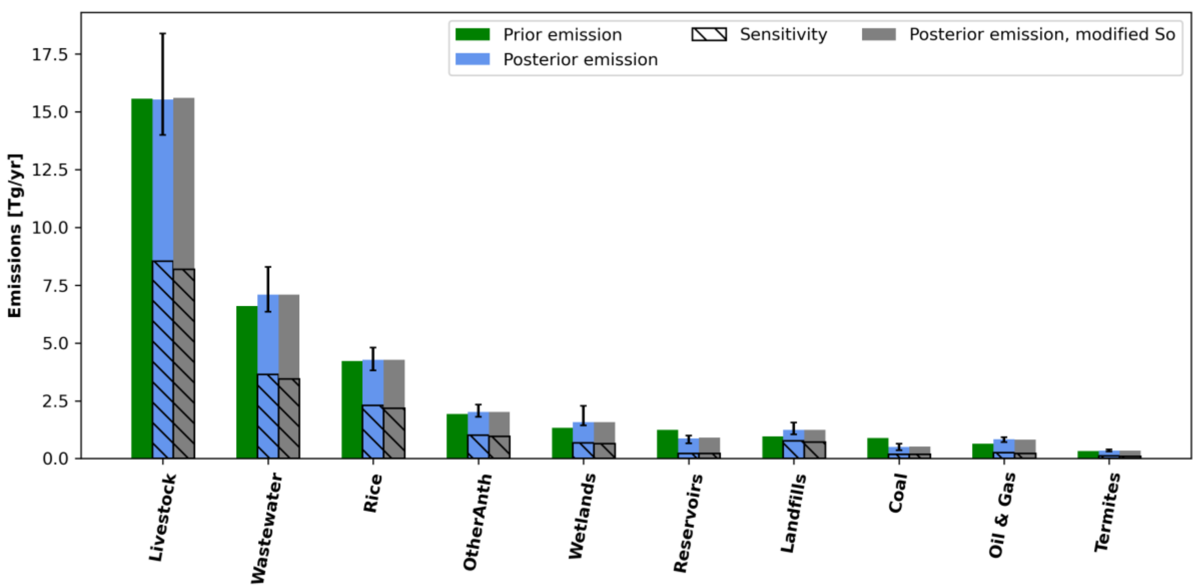

Figure R3. Prior and posterior emissions from the base inversion and posterior emission from the inversion using the modified super-observational error for different emission sectors over India in 2021. The error bars represent the ensemble range. The sensitivity for each sector is derived using the averaging kernel, shown as hashed bars that cover a fraction of the emission bars. Sensitivities for the modified inversion are slightly lower because of the larger *observational uncertainties, but emission results are consistent and clearly within the uncertainty ranges provided by the ensemble.*

To further assess the sensitivity to the observation-error specification, we performed an additional inversion using a constant super-observation error variance of (11.23 ppb)^2 instead of the original spatially and temporally varying values. This experiment produced a posterior national methane emission of 35.3 Tg/yr, which lies within the uncertainty estimate of our uncertainty ensemble. The largest increases were found in rice, wastewater, wetlands, and other anthropogenic emissions, while coal mine emissions again decreased from the prior values (from 0.9 to 0.4 Tg/yr, Figure R4). These estimates are well within the uncertainty range of our national and coal-specific emission estimates, demonstrating that the principal conclusions of the study are robust to the choice of observation-error specification.

These sentences have been added at Line 346 and Line 465:

"We conduct a sensitivity test using an additional residual-fitting analysis based on Eq. (6) for observations over India. This yielded $r_{retrieval} = 0.59$, $\sigma_{transport} = 4.4$ ppb, and $\sigma_{retrieval} = 16.5$ ppb, resulting in a mean super-observation error variance of (12.6 (10.4-16.4) ppb)^2, close to the value used in the base inversion. An additional sensitivity test using a constant super-observation error variance of (11.23 ppb)^2 is performed to assess the uncertainty associated with super observation errors."

"The sensitivity test using the super-observation error derived from residual fitting produced posterior emissions and the sectoral emissions that are consistent with the base inversion. Using a constant super-observation error variance of (11.23 ppb)^2, increased the estimated emissions by 0.8 Tg yr^{-1} relative to the base inversion, remaining within the uncertainty range. The largest increases occurred in rice, wastewater, wetlands, and other anthropogenic emissions, whereas coal mine emissions decreased from 0.9 to 0.4 Tg yr^{-1}, consistent with the base inversion. These sectoral changes also remained within the estimated uncertainty ranges."

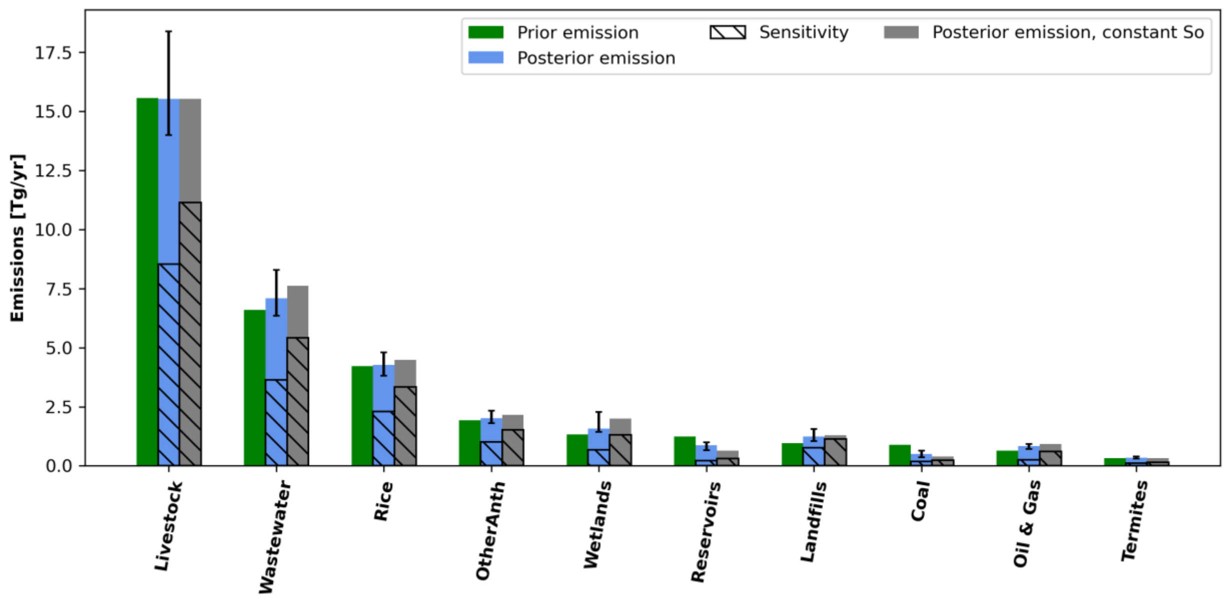

Figure R4. Same as Figure 3 but for posterior emission derived using the constant super observation error (11.23 ppb)^2.

2. Aerosol contamination is addressed only by excluding "hazy days"; partial / sub-pixel aerosol coverage in the non-monsoon season is the larger, unaddressed problem

The hazy-day exclusion (63 days, heavily clustered in late October and November) does not address spatially heterogeneous, partial aerosol and cloud contamination on ordinary days across the long non-monsoon period. This matters for two reasons. First, aerosol-induced biases in the 2.3 µm window can be large and sign-dependent on aerosol type and surface albedo, and they are now shown to be specifically enhanced in the presence of aerosols (Somkuti et al., 2025; Huang et al., 2020; Lorente et al., 2023); the magnitude and sign of this effect depend on absorbing-aerosol optical properties that vary strongly across polluted Asian regions and are themselves uncertain (Wang et al., 2021; Guan et al., 2026). Second, the most-affected regions, namely the Indo-Gangetic Plain and the eastern coal belt (Odisha and Jharkhand), coincide with the most consequential corrections. The blended product (Balasus et al., 2023) corrects some biases via machine learning but does not eliminate aerosol-driven errors, and the residual structure is not characterized here. I recommend a sub-scene or per-pixel AOD screening test rather than day-level exclusion alone, an analysis of how residual aerosol bias propagates into sectoral attribution, and explicit acknowledgement that this is a leading uncertainty for the northern-India and coal results.

Author Response:

As requested by the reviewer, we performed two sensitivity analyses using stricter pixel-wise aerosol filtering using the aerosol optical thickness (AOT) included in the level-2 TROPOMI methane product: (1) SWIR AOT < 0.13 with quality assurance value = 1.0, and (2) SWIR AOT < 0.06 with quality assurance value = 1.0.(Apituley, 2022) The base inversion only uses quality assurance value equals 1.0, which is the recommended filtering of the TROPOMI methane data.

Using the SWIR AOT < 0.13 filter, the posterior methane emission was estimated to be 34.5 Tg/yr, which is 0.1 Tg/yr higher than the base inversion estimate of 34.4 Tg/yr (32.0–40.4 Tg/yr). This difference lies well within the uncertainty range of the base inversion. Relative to the base inversion, emissions increased by approximately 1–12%, primarily over western India, including Rajasthan and parts of central and eastern India and such changes lie within the uncertainty range (Figure R5). The sectoral emission estimates also remained consistent with the base inversion within their associated uncertainty ranges (Figure R6).

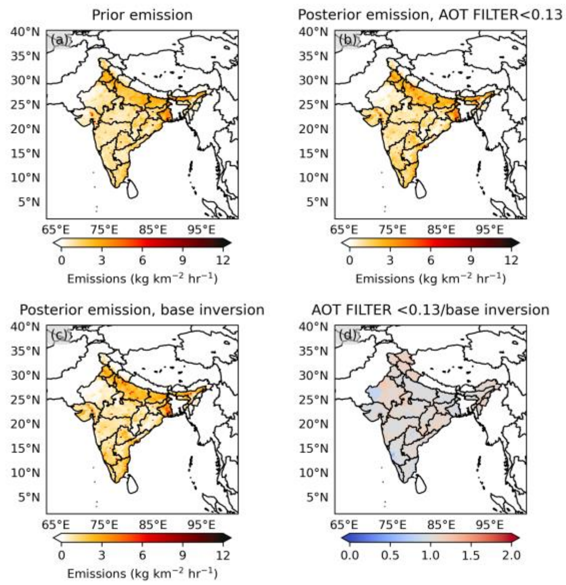

Figure R5. Same as Figure 2 but for the posterior emissions derived using quality assurance value = 1.0 + aot_filter<0.13.

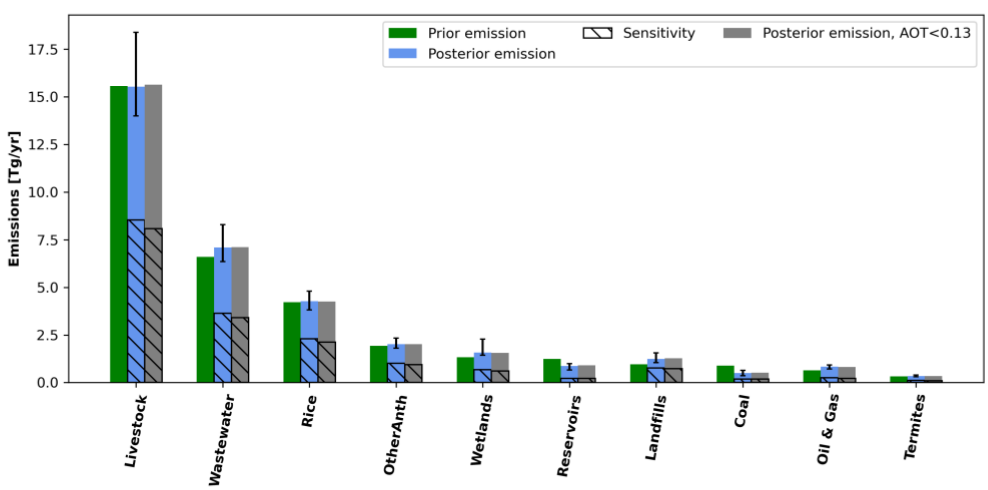

Figure R6. Same as Figure 4 but comparing the base inversion with emissions derived with aot filter <0.13.

Applying the more stringent SWIR AOT < 0.06 filter resulted in a posterior emission estimate of 33.8 Tg/yr, which is 0.6 Tg/yr lower than the base inversion but still falls within its uncertainty range. The stricter filtering substantially reduced the number of super-observations, limiting observational coverage across the study domain. Consequently, localized changes in scaling factors were observed, particularly over the northern tip of India, where methane emission sources are minimal (Figure R7). The largest spatial differences occurred over central India (Maharashtra and Chhattisgarh), western India (Rajasthan and Gujarat), and southern India (Karnataka), whereas only minor changes were observed over the Indo-Gangetic Plain and eastern India. The changes observed across these regions and states remain within the uncertainty ranges of the base inversion. Similarly, sectoral emission estimates, including those for major source sectors such as coal mining, remained within the uncertainty range of the base inversion (Figure R8)

Overall, these sensitivity analyses demonstrate that the national, and sectoral posterior emissions are robust to stricter pixel-wise SWIR AOT filtering. Although localized differences are observed, particularly over central and western India, no substantial changes occur over the Indo-Gangetic Plain or eastern India, where the largest emission corrections are inferred. We have added sentences at Line 345 and Line 451 addressing these additional analyses:

"The base inversion uses observations with quality assurance value equals 1.0, which is the recommended filtering of the TROPOMI methane data (Apituley, 2022). Additionally, we performed two sensitivity analyses using stricter additional pixel-wise aerosol filtering using the aerosol optical thickness (AOT) included in the level 2 TROPOMI methane product: SWIR AOT < 0.13 and SWIR AOT < 0.06."

"Using the additional SWIR AOT filters of <0.13 and <0.06 yielded posterior methane emissions of 34.5 and 33.8 Tg yr^{-1}, respectively, compared with 34.4 (32.0–40.4) Tg yr^{-1} in the base inversion. These differences of +0.1 and −0.6 Tg yr^{-1} remained within the base inversion's uncertainty range, with sectoral emissions, including major sources such as coal mining, also remaining within their respective uncertainty ranges."

Nevertheless, residual aerosol-related retrieval biases remain an important source of uncertainty for methane inversions over northern India and other regions with persistently high aerosol loading. To explicitly acknowledge this limitation, we have added the following statement to the manuscript (Line 821):

"The Indo-Gangetic Plain and eastern India frequently experience elevated aerosol loading. Therefore, future analyses should further evaluate the impact of residual aerosol effects on methane emission estimates, particularly in cities where aerosol-related uncertainties may be more pronounced. Such analyses could help quantify the contribution of residual aerosol effects to uncertainties in inferred methane emissions."

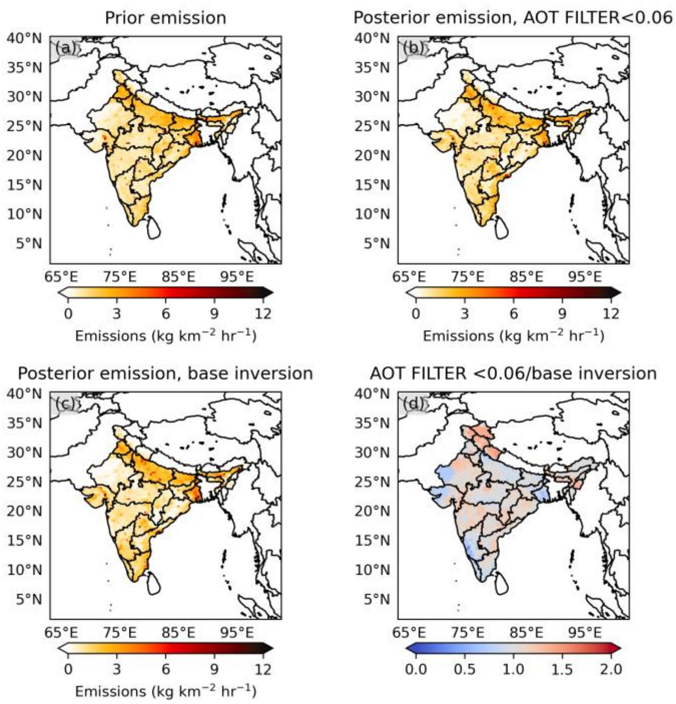

Figure R7. Same as Figure 2 but for the posterior emissions derived while using quality assurance value = 1.0 + aot_filter<0.06.

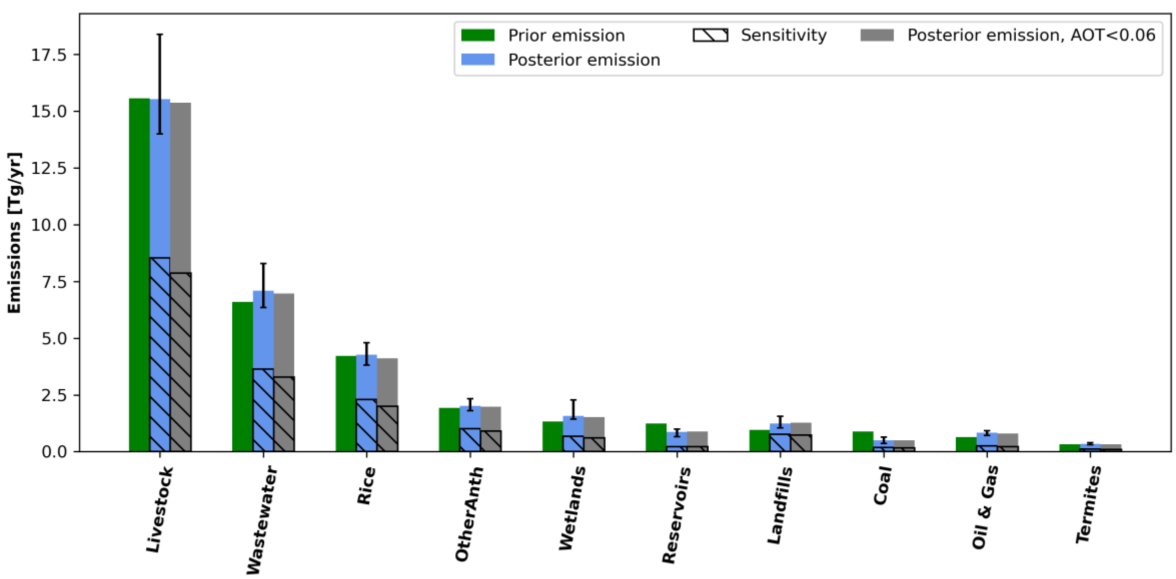

Figure R8. Same as Figure 4 but comparing the base inversion with emission derived with aot filter <0.06.

3. The −57% coal correction is presented more confidently than the evidence supports

This is the most striking sectoral result, and it currently rests on assumptions that should be reconciled. First, regarding prior dependence, the sectoral attribution (Sect. 2.8) assumes that grid-cell-level relative sectoral contributions in the prior are accurate. With a total DOFS of 296 over roughly 1785 elements, the split carries substantial prior information, and coal, although spatially concentrated, is co-located with the heaviest aerosol loading discussed in point 2. The coal prior itself derives from national UNFCCC-based reporting via GFEI (Scarpelli et al., 2020), so the inversion is correcting a specific bottom-up construction rather than an independent baseline. Second, regarding the direction-of-evidence tension, independent work has repeatedly found Chinese and global coal-mine methane to be under-reported or revised in complex directions (Sadavarte et al., 2021; Gao et al., 2021), so a large downward correction warrants engagement with that literature rather than a one-sided surface-mining argument. Third, the proposed mechanism, namely a shift toward less methane-intensive surface mining not yet reflected in activity data (Wright et al., 2024), is plausible but is not a demonstration, and the competing explanation, in which aerosol-contaminated retrievals over the coal belt are read as an emission reduction, is not ruled out. I recommend independent corroboration, whether facility-level, isotopic, or in-situ, or else substantial hedging, before the coal claim is stated as strongly as it is in the abstract.

Author response:

The original manuscript already included a discussion of limitations in the Conclusions (Lines 659–665), including the dependence of sectoral attribution on the prior source distribution and the lack of facility-scale observations for the coal sector and has been retained in the modified manuscript at Line 794. Additionally, such limitations are further discussed at Line 650:

“The breakdown of prior emissions shows a large variety of sources contributing. The emission breakdowns discussed here are based on mapped bottom-up inventories (mainly EDGAR v7 and GFEI), supplemented with GHGSat data for landfills. These come with significant uncertainty, and the resulting urban estimates are not always in agreement with local greenhouse gas inventories, as for example compiled by cities.”

We have also modified the Line 323:

“This attribution method relies on the grid-cell-level relative sectoral contributions from the prior taken from EDGAR and GEFI and assumes that sources are evenly distributed within the grid cells.”

To avoid overstating our findings, we have revised the Abstract and now emphasize the need for additional local observations. Specifically, we added the statement that “These results illustrate how satellite-based analyses can inform methane mitigation while highlighting the need for additional local observations” (Lines 34–35). The potential impact of aerosol optical depth (AOD) has been addressed in our response to the previous comment.

To better explain the inferred reduction in coal-related methane emissions, we have added the following discussion (Line 614), which removes strong statements on the reasons underlying the lower coal mining emissions that we find:

“The prior national-level coal-mine emissions from Scarpelli et al (2020) are based on India's UNFCCC inventory, which applies the IPCC Tier-2 methodology using country-specific emission factors from Singh and Kumar (2016). Emission factors for underground mines are categorized according to the degree of gassiness, whereas a single emission factor is applied to all surface mines despite differences in mine characteristics, introducing uncertainty in the estimated emissions. By 2018, approximately 94% of India's coal production came from surface mines and only 6% from underground mines, reflecting a substantial shift over the past two decades (Sadavarte et al., 2022). Previous studies have reported both overestimation (Sadavarte et al., 2021) and underestimation (Gao et al., 2021; Sadavarte et al., 2022) of bottom-up coal mine emission estimates, largely due to uncertainties in emission factors."

4. Validation is weak and only partially independent

The GOSAT evaluation (Fig. 2, S7) is not independent, because GOSAT is the reference used to construct the blended product that is assimilated (Balasus et al., 2023), and this should be stated plainly where the GOSAT comparison is presented. Even so, it retains large structure, with monthly differences of roughly −30 to −40 ppb in summer that far exceeds the approximately 11 ppb assumed observation error, which points to seasonally varying model and retrieval error not represented in the annual, spatially uniform error treatment. The single surface site at Nainital shows only marginal improvement, from an MAE of 73.3 to 70.5 ppb, with individual residuals exceeding 200 ppb. While representation error explains much of this, given that a 0.25° column-oriented inversion is compared against weekly flasks at a mountain site (Nomura et al., 2021), that is precisely why one such site cannot constitute validation. I recommend genuinely independent evaluation, such as additional in-situ records or a withheld-data cross-validation.

Author response:

We consider the comparison with GOSAT to be the best available evaluation because no other suborbital observations are available and the inversion assimilates the blended methane product rather than GOSAT observations directly. GOSAT is only used indirectly in the construction of the bias correction of the blended product (Balasus et al., 2023), the TROPOMI+GOSAT product is primarily derived from TROPOMI observations.

Regarding the summer differences, the prior simulation exhibits monthly mean biases of approximately −30 to −40 ppb relative to GOSAT, which are reduced to approximately −25 to −20 ppb in the posterior simulation. During the Indian monsoon season (June–August), persistent cloud cover substantially reduces the number of useful TROPOMI observations, limiting the observational constraints available to the inversion. At the same time, this also means the GOSAT-derived biases are based on relatively few and non-uniform observations. We acknowledge that the remaining summer differences likely reflect a combination of reduced observational coverage and seasonally varying retrieval and model errors as explained at Line 339.

For the Nainital comparison, we agree that a single surface site cannot provide comprehensive validation of the inversion. The annual MAE improves modestly (73.3 to 70.5 ppb), largely because Nainital has limited TROPOMI observations and because representation errors are expected when comparing a coarser (0.25°) model grid with point measurements at a mountain site. Nevertheless, during March–September, when TROPOMI observations are more frequent, the mean bias improves from −7.8 ppb to 3.0 ppb, explained in Line 345. To explain such differences, we added an additional sentence at Line 412:

"The relatively large differences between the model simulations and surface observations at Nainital may partly reflect the complex mountainous terrain surrounding the station. The point measurements are influenced by local-scale processes and topographic effects that may not be fully resolved by the relatively coarse-resolution transport model, potentially contributing to the observed discrepancies."

To the best of our knowledge, Nainital is the only publicly available in-situ methane dataset for India for 2021. We performed an additional evaluation of the TROPOMI-based inversion using GOSAT observations. We think this is preferred to evaluating based on a subset of the TROPOMI data themselves through withheld-data cross-validation. The limited availability of independent observations and the need for a more comprehensive and systematic national in-situ methane monitoring network were already acknowledged in the original manuscript (Conclusions, Lines 663–666) and have been retained in the revised manuscript. This need is now also highlighted in the Abstract.

5. Annual-mean optimization and imposed seasonality limit diagnosis of the above

Optimizing annual 2021 emissions with EDGAR-imposed seasonality, combined with the substantial boundary-condition adjustments shown in Fig. S5, leaves little freedom to absorb seasonally structured mismatch as model and retrieval error rather than as emissions, which raises the risk of aliasing. The use of nested GEOS-Chem with annual-mean optimization follows established practice (Varon et al., 2022; Chen et al., 2022), but the interaction between the annual-mean framing and the seasonally varying aerosol bias of point 2 should be discussed. Please also clarify the temporal sampling of the super-observations, since the text emphasizes spatial aggregation while leaving unstated both the per-cell temporal sampling and whether super-observations are formed per overpass.

Author Response*:*

We acknowledge that optimizing annual mean emissions while prescribing the EDGAR seasonal profile does not allow the inversion to resolve seasonal emission variability. This limitation is discussed in the Conclusions (Lines 686–688) at original manuscript and has been retained in the revised manuscript (Line 805). As noted in our response to Comment 2, the potential influence of seasonally varying aerosol-related retrieval biases has also been addressed.

To further assess the sensitivity of our results to the treatment of boundary conditions, we performed an additional inversion without monthly boundary-condition optimization. The resulting national methane emission was 34.7 $Tgyr^{-1}$, differing by only 0.3 $Tgyr^{-1}$ from our baseline estimate and remaining well within the reported uncertainty range. Likewise, the inferred sectoral emissions also remained within their respective uncertainty ranges. These results indicate that our national and sectoral emission estimates are robust to the temporal treatment of the boundary conditions.

To address the monthly boundary condition impact, the sentence has been added at Line 351 and Line 469:

"To further assess the sensitivity of our results to the treatment of boundary conditions, we performed an additional inversion without monthly boundary-condition optimization."

"A sensitivity test without monthly boundary-condition optimization yielded national methane emissions of 34.7 $Tgyr^{-1}$, only 0.3 $Tgyr^{-1}$ higher than the baseline estimate and well within its uncertainty range. Sectoral emissions likewise remained within their respective uncertainty ranges, demonstrating the robustness of our national and sectoral estimates to the treatment of boundary conditions."

Regarding the temporal sampling of the super-observations, we have clarified the methodology in the revised manuscript (Lines 153–157) as follows:

"TROPOMI observations are averaged over the GEOS-Chem resolution of 0.25° x 0.3125° as described by Chen et al. (2023) and Estrada et al. (2025), resulting in 888987 super-observations across our domain in 2021 (Figure 1). Super-observations are generated by averaging all valid TROPOMI retrievals within each GEOS-Chem grid cell for each satellite orbit (Figure 1 and Figure S1). These aggregated observations are referred to as super-observations because averaging multiple retrievals reduces the random observational error relative to individual measurements."

6. Homogenization of emission signals

The original daily and grid-level satellite observations were spatially aggregated for the assimilation and inversion analysis. Although this approach reduces random observational uncertainties, it leads to homogenization of emission signals: strong emission hotspots tend to be underestimated while weak emission areas are overestimated. Even if the total emission of each aggregated grid remains unchanged, the spatial characteristics of local emissions are distorted, which adversely affects the high-resolution emission analysis at state and city levels. The authors have not analyzed or discussed this issue.

Author Response:

We agree that constructing super-observations by averaging TROPOMI retrievals within each GEOS-Chem grid cell reduces random observational errors and smooths sub-grid variability. In the IMI framework, we assimilate observations at the model resolution, and emission optimization is performed at the same GEOS-Chem resolution. Therefore, the variability of individual TROPOMI retrievals within a grid cell inherently cannot provide additional information on the spatial distribution of emission sources. When it comes to the breakdown of emissions per sector, we rely on the prior breakdown of emissions for individual grid cells as clarified in at Line 331:

"This attribution method relies on the grid-cell-level relative sectoral contributions from the prior taken from EDGAR and GFEI and assumes that sources are evenly distributed within the grid cells."

Furthermore, our inversion uses a lognormal error, which is better suited to capture high tailed methane emissions at the grid-cell level rather than normal-errors as explained at Lines 256 to 259. We also compared posterior emissions derived using both lognormal and normal error and found that they agree within their uncertainty ranges. The normal-error inversions are included as ensemble members to quantify the posterior uncertainty.

7. The use of GHGSat estimates as annual prior emissions require justification

The authors use instantaneous GHGSat landfill emission estimates from 2021–2022 to modify the annual prior emissions for the 2021 inversion, but it is unclear how a limited number of satellite observations can represent annual mean emissions. The authors should report the number of observations, detections and non-detections, individual emission estimates, and associated uncertainties for each landfill, and justify the use of 2022 observations to represent 2021 emissions. In addition, setting EDGAR landfill emissions within 25 surrounding grid cells to zero and concentrating the GHGSat estimate into a single grid cell may remove other unobserved small or diffuse waste sources and artificially alter the prior spatial distribution. Sensitivity tests using alternative replacement strategies and an inversion without GHGSat-based prior adjustments are needed. Because GHGSat information is already incorporated into the prior, agreement between the posterior and GHGSat estimates should not be presented as independent validation. The conclusions regarding the improved separation of landfill and wastewater emissions should therefore be stated more cautiously.

Author Response:

We have added a supplementary table Table S1 summarizing the number of GHGSat observations, mean methane emission rates, associated uncertainties, and observation years for all 18 landfill sites used in this study (Table S1). The underlying GHGSat dataset, including individual emission estimates for each observation, is publicly available in the repository https://zenodo.org/records/16641834 provided by Dogniaux et al. (2025). Here, we report the available mean emission rates and associated uncertainties for each landfill. All available GHGSat observations reported for the Indian landfills during 2021–2022 featured plume detections. Of the 18 landfills, nine have mean emission rates available for both 2021 and 2022, and these estimates are statistically consistent between the two years. Therefore, to increase the number of observations and obtain more robust emission estimates, we use the mean emission rates derived from observations collected during 2021–2022 for all 18 landfills, using the available observations for each site. A sentence has been added on this in Line 219:

"Of the 18 landfills, nine have mean emission rates available for both 2021 and 2022, and these estimates are statistically consistent between the two years. Therefore, to increase the number of observations and obtain more robust emission estimates, we use the mean emission rates derived from all observations collected during 2021–2022 for all 18 landfills. The underlying GHGSat dataset is publicly available in the repository https://zenodo.org/records/16641834 provided by Doginaux et al. (2024)."

Table R1. GHGSat based 2021-2022 estimations for 18 landfills over India.

latitude	**longitude**	**city/town/village/county**	**state**	**country**	**NDaySat_total**	**Q_mean_total**	**Uncert_mean_total**	**year**
22.9826239	72.5688882	Piplaj	Gujarat	India	25	3.61	0.36	2021-2022
28.7427763	77.15524683	Alipur Tehsil	Delhi	India	2	1.29	0.42	2022
28.622714745000003	77.3260399	Mayur Vihar Tehsil	Delhi	India	32	2.53	0.25	2021-2022
28.509638	77.28408118499999	Kalkaji Tehsil	Delhi	India	2	2.20	0.74	2021
21.10697853724138	72.80562677275863	Majura Taluka	Gujarat	India	25	2.89	0.36	2021-2022
22.23300505904762	73.20675647904761	Vadodara Rural Taluka	Gujarat	India	22	0.82	0.13	2022
28.4026139	77.1719354	Gurugram District	Haryana	India	10	1.45	0.24	2021-2022
22.536251478181818	88.42410893363636	Kolkata	West Bengal	India	10	1.69	0.38	2021-2022
22.563346	88.4444196	Bidhannagar	West Bengal	India	10	0.09	0.09	2021-2022
19.124134020909096	72.95264296318182	Mumbai	Maharashtra	India	22	9.05	1.473	2021-2022

19.0703417	72.9297917	Mumbai	Maharashtra	India	16	0.31	0.16	2021-2022
18.4714568	73.9509378	Manter Wadi	Maharashtra	India	11	0.78	0.110	2022
30.929333333333336	75.90706666666667	Ludhiana	Punjab	India	5	0.61	0.28	2022
17.518098326956522	78.59313989869564	Dammaiguda	Telangana	India	23	6.91	0.94	2021-2022
13.1352049	80.2677878	Chennai	Tamil Nadu	India	2	1.74	0.60	2022
12.9530163	80.22445982250001	Sholinganallur	Tamil Nadu	India	4	3.53	1.149	2022
26.4490174	80.2346042	Kanpur	Uttar Pradesh	India	15	0.60	0.268	2022
26.79697802235294	80.78149945588235	Sarojani Nagar	Uttar Pradesh	India	15	1.64	0.2645	2022

The incorporation of the GHGSat data in the prior inventory features the best available information on the location of waste-related emissions. We performed a sensitivity analysis using the original EDGAR v7 landfill emissions instead of the GHGSat-adjusted prior. Recomputing the Jacobian matrix for a different prior is computationally expensive. We therefore applied the prior-swapping method developed by Cusworth et al. (2021), which enables posterior emissions to be recalculated for an alternative prior using the Jacobian matrix derived from the base inversion. In this method, the optimal estimate ($\hat{z}$) and its error covariance ($\hat{Z}$) are derived from the optimized fluxes ($\hat{x}$) and their covariances ($\hat{S}$), without relying on inventory-based relative sector weightings.

$$\hat{z} = z_A + \hat{\mathrm{Z}}\mathrm{M}^T\hat{\mathrm{S}}^{-1}\left[\left(\mathrm{I} - \hat{\mathrm{S}}\mathrm{S}_{\mathrm{A}}^{-1}\right)(x_a - \mathrm{M}z_A) + (\hat{x} - x_a)\right] \quad (1)$$

Where z_A is the swapped prior emission fluxes, M is an aggregation matrix summing emissions to fluxes, x_a is the prior emission fluxes, I is the identity matrix, $\mathrm{S_A}$ is the prior error covariance matrix. The posterior emission error covariance matrix $\hat{\mathrm{Z}}$ is then calculated as follow:

$$\hat{\mathrm{Z}} = \left(\mathrm{M}^T\left(\hat{\mathrm{S}}^{-1} - \mathrm{S}_{\mathrm{A}}^{-1}\right)\mathrm{M} + \mathrm{Z}_{\mathrm{A}}^{-1}\right)^{-1} \quad (2)$$

Using the original EDGAR v7 landfill emissions, the optimized national methane emission is estimated to be 34.3 Tg yr^{-1}, consistent with the base inversion (34.4 (32.0 – 40.4) Tg yr^{-1}), and within the reported uncertainty range. At the national sectoral level, posterior landfill emissions decrease by approximately 42% relative to the base inversion (1.3 (1.1 – 1.6) Tg yr^{-1}), with a corresponding increase in wastewater emissions of 0.3 Tg/yr. However, the increase in wastewater emissions remains within the estimated uncertainty range. The largest differences are observed over major urban areas as shown in Figure R9. Among the 14 cities analyzed, posterior total emissions derived using the EDGAR v7 prior are 15–42% lower than the base inversion in Surat, Mumbai, and Hyderabad, while the remaining cities agree within their uncertainty range (Figure R10). Overall, the sensitivity analysis indicates that EDGAR v7 likely underestimates landfill methane emissions in 10 of the 14 cities (Figure R11). Of the 14 cities, 11 have independent GHGSat landfill emission estimates, and except for Kolkata, the posterior landfill emissions derived using the EDGAR v7 prior are factor 1.6 to 7.5 lower than the GHGSat estimates, with largest difference observed over Chennai (Figure R11). The lower landfill emissions are largely compensated by increased wastewater emissions (Figure R12), as wastewater serves as the background emission source and is spatially co-located with landfill emissions in urban areas and is strongly spatially correlated within

EDGAR. This sensitivity analysis demonstrates that incorporating GHGSat landfill estimates into the prior reduces the spatial correlation between landfill and wastewater emissions, thereby improving their separation in the inversion.

Regarding the inversion with EDGAR v7 landfill emissions, we added the results at Line 361, Line 680 and Line 815:

"To evaluate the impact of the incorporation of the GHGSat data in the prior inventory, we perform a sensitivity analysis using the original EDGAR v7 landfill emissions. To prevent having to recompute the full Jacobian, we applied the prior-swapping method developed by Cusworth et al. (2021)."

"The sensitivity analysis using EDGARv7 landfill emissions resulted in 15–42% lower total emissions than the base inversion in Surat, Mumbai, and Hyderabad, while the remaining cities agree within their uncertainty range (Figure S33)."

"Overall, the sensitivity analysis indicates that EDGAR v7 likely underestimates landfill methane emissions in 10 of the 14 cities. Of the 14 cities, 11 have independent GHGSat landfill emission estimates, and except for Kolkata, the posterior landfill emissions derived using the EDGAR v7 prior are factors 1.6 to 7.5 lower than the GHGSat estimates, with the largest difference observed over Chennai (Figure S36). The lower landfill emissions are largely compensated by increased wastewater emissions, as wastewater serves as the background emission source and is spatially co-located with landfill emissions in urban areas, especially in EDGAR's emission maps (Figure S37)."

To clarify the independent validation part, we have modified the caption in Figure 8 as follow:

"In the caption of Figure 8, we have further clarified that the comparison with GHGSat data is not an evaluation of the results but rather supports the interpretation of the inversion output and compares the TROPOMI-based and GHGSat-only estimates."

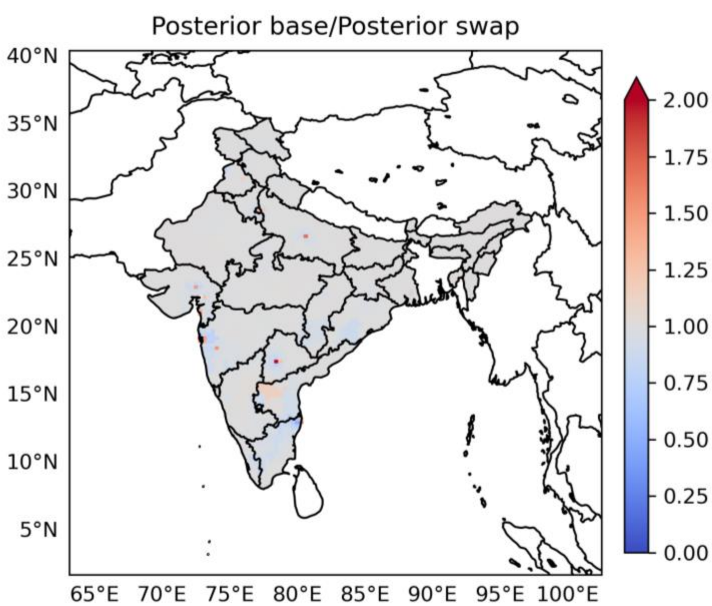

Figure R9. Ratio of posterior methane emissions derived from the base inversion to posterior emissions obtained after replacing the GHGSat-adjusted landfill prior with the original EDGAR v7 landfill emissions.

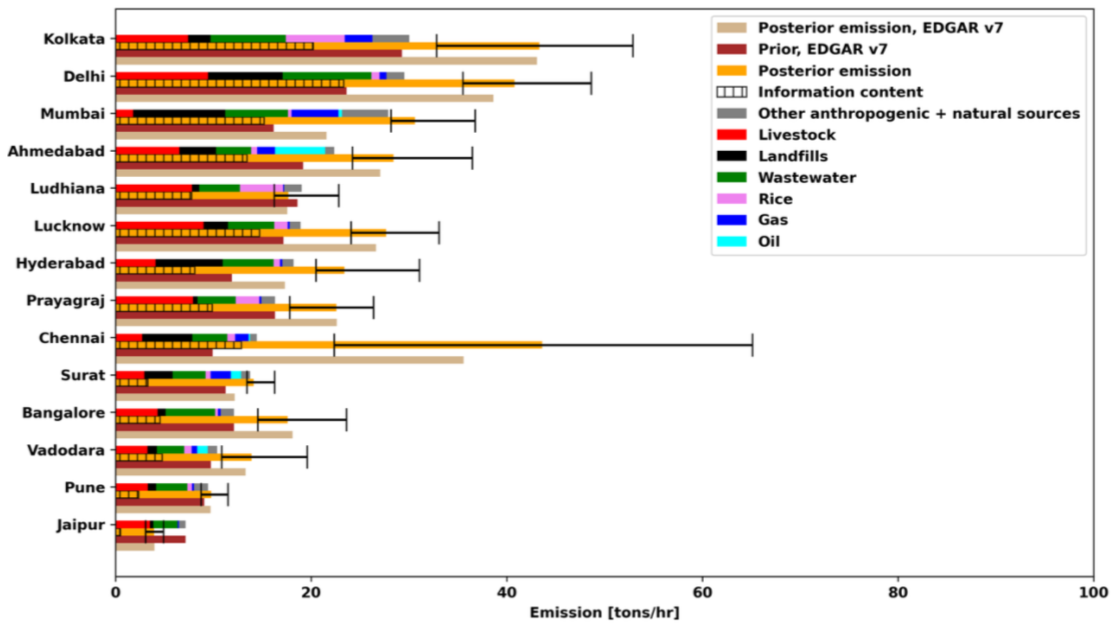

Figure R10. Comparison of prior emissions with sectoral contributions and posterior emissions derived across 14 Indian cities. Total prior and posterior emissions are calculated as the cumulative sum of emissions across nine grid cells surrounding each city center. Error bars represent the uncertainty derived from the 35-member ensemble. The sensitivity for each city is derived from the averaging kernel, represented by bars with hashed patterns shown as a fraction of the emissions. These sensitivities are a measure for the extent to which the posterior emission estimates are constrained by the satellite observations.

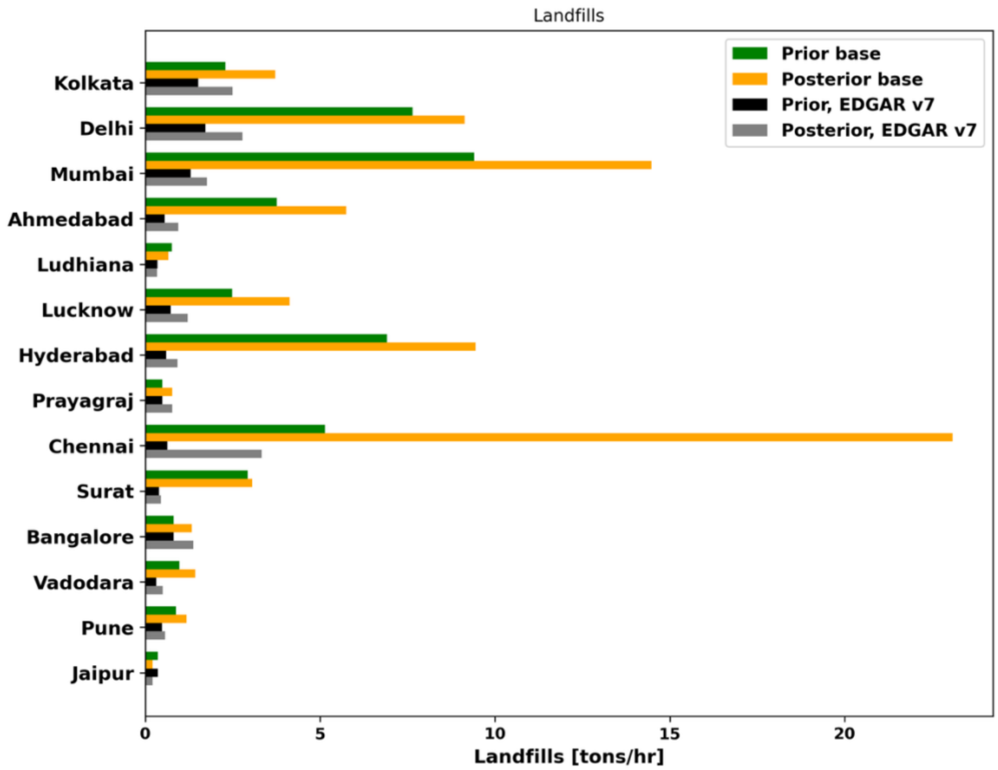

Figure R11. Same as Figure R10 but for landfill emissions.

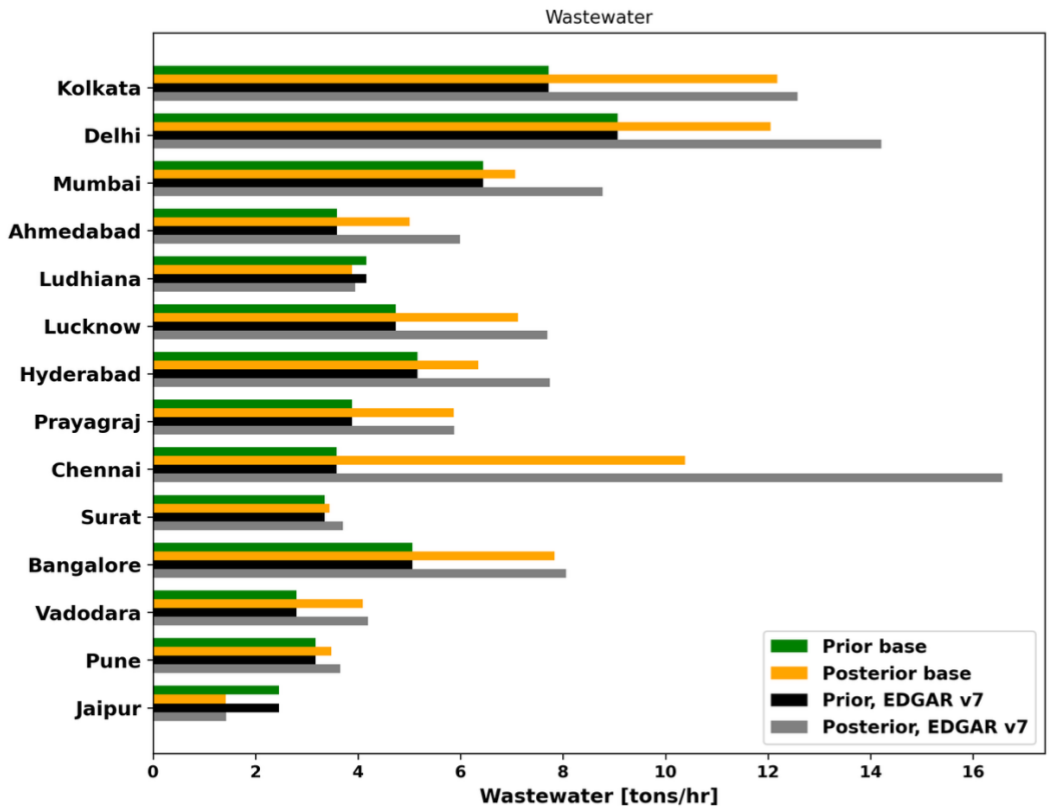

Figure R12. Same as Figure R10 but for wastewater emissions.

Specific comments

EQ 6 in Sect. 2.7. Report the spatial distribution of the super-observation error and the number of super-observations per grid cell, since the domain total of 888,987 implies tens per cell per year, which would dispel any impression of heavy temporal aggregation.

Author Response:

As suggested by the reviewer, we have added supplementary figures Figure S1 showing the spatial distribution of the number of super-observations and the corresponding mean super-observation error for each GEOS-Chem grid cell (Figures R13). These figures demonstrate that each grid cell is constrained by multiple super-observations throughout the year, rather than by a single temporally averaged observation. As mentioned above, we have also clarified that no temporal aggregation of observations takes place.

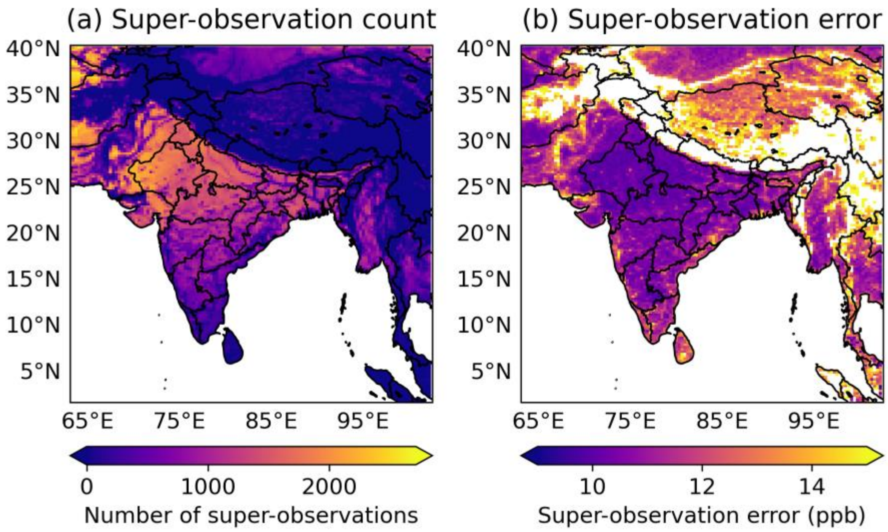

Figure R13. Number of super observation count (a) and associated annual mean super observation error derived using the equation 6.

Fig. S4. Individual grid points worsening after inversion should not be over-interpreted, because with = 0.1 the inversion deliberately does not fully fit the observations (regularized cost function; Brasseur and Jacob, 2017), so local degradation alongside an improved aggregate correlation, which rises from 0.89 to 0.93, is expected. I raise this so that the authors can pre-empt it.

Author response:

Figure S4 (now Figure S23) demonstrates an overall improvement in agreement between the posterior simulation and TROPOMI observations, as indicated by the increase in spatial correlation from 0.89 to 0.93 together with reductions in mean bias and RMSE. The performance of the inversion should therefore be assessed using these overall statistical metrics rather than individual scatter points. The sentence at Line 353 has been modified as follow:

"The mean bias over India using TROPOMI super-observations decreases from 2.1 ppb to 0.3 ppb and the RMSE is reduce from 14.3 to 11.7 ppb while the correlation coefficient (r) improves from 0.89 to 0.93 (Figure S23), demonstrating an overall improvement in agreement between the posterior simulation and the observations."

Sect. 2.9. Report the sectoral, and not only the total, sensitivity to hazy-day exclusion, since the text gives only the +0.7 Tg yr^{-1} total change.

Author Response:

The sentence has been modified at Line 498: "Excluding hazy days increases the estimated emissions by approximately 0.7 Tg yr^{-1} relative to the base inversion. This increase falls within the estimated uncertainty range. Most of the increase is attributed to the livestock sector (+0.5 Tg yr^{-1}), followed by wastewater (+0.1

Tg yr⁻¹) and landfills (+0.1 Tg yr⁻¹), while emissions from the other source sectors equal the base inversion. All sectoral estimates remain within the uncertainty ranges of our base posterior estimates."

Sect. 3.4 (Talcher coal field). The factor-6.5 local reduction rests on a few grid cells in a high-aerosol region, so please show the averaging-kernel sensitivity and aerosol conditions for these cells.

- As per reviewer request, aerosol optical thickness and averaging kernel sensitivity has been added in the supplementary Figure S32. At Line 616, the sentence has been added as follow:

"Figure S32 shows the no local aerosol effects over the Talcher coal field. The prior coal-mine emissions from Scarpelli et al (2020) are based on India's UNFCCC inventory, which applies the IPCC Tier-2 methodology using country-specific emission factors from Singh and Kumar (2016)."

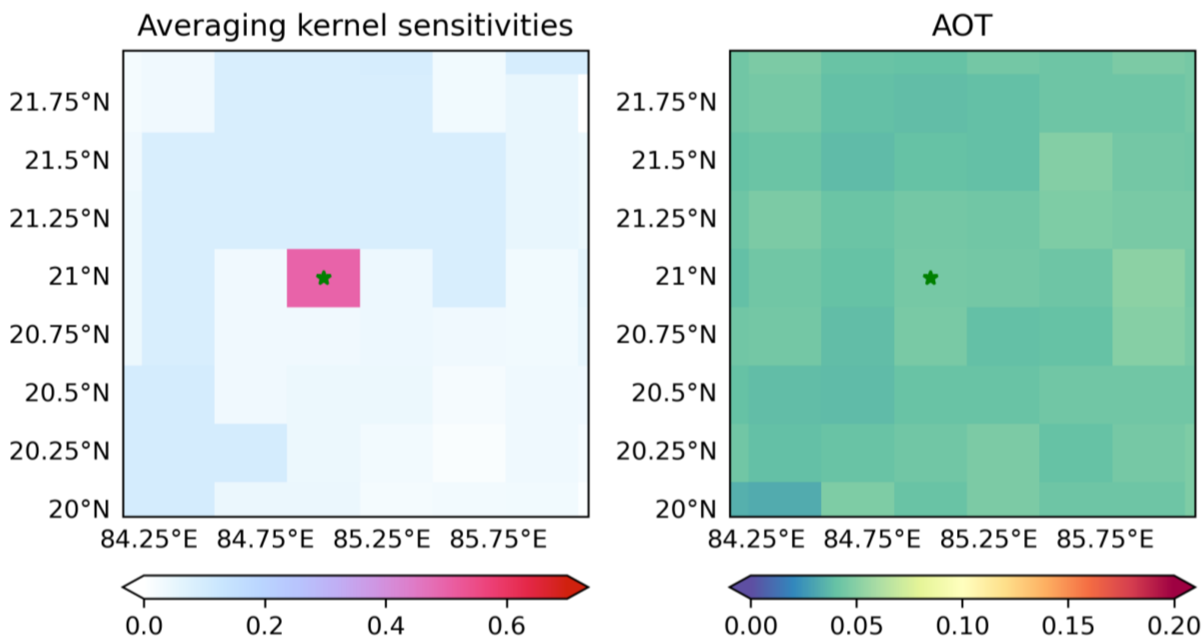

Figure R14. Averaging kernel sensitivity and Aerosol Optical Thickness (AOT) around the Talcher coal field in Odisha (20.977 ° N, 85.137 ° E). India.

Figure S7 presents the monthly mean biases between inversion simulations and GOSAT observations, with the maximum monthly bias approaching 10 ppb. The actual biases of daily and individual grid observations are inevitably larger than this monthly average value, exceeding the preset observational error range in the manuscript.

Author response:

The TROPOMI observation error of $(11.23\ \text{ppb})^2$ is based on super-observations, whereas the GOSAT and model difference is evaluated at the grid level. Therefore, these two quantities are not directly comparable. Furthermore, the inversion is constrained by TROPOMI observations, while the GOSAT comparison provides an evaluation of the posterior simulation. To clarify this distinction, we have revised the text (Line 402) and added error bars representing one standard deviation of the monthly model–GOSAT differences in Figure S26.

"Figure S26 presents the monthly mean differences between the inversion simulations and GOSAT observations, with error bars representing one standard deviation of the collocated model–GOSAT differences. The monthly mean differences for the prior simulation ranges from 1.4 ppb to −40.0 ppb, with the largest negative differences occurring during summer. The inversion reduces these differences to a range of −0.3 ppb to −25.0 ppb, although relatively larger differences persist during June–August because of the limited TROPOMI and GOSAT observational coverage during this period."

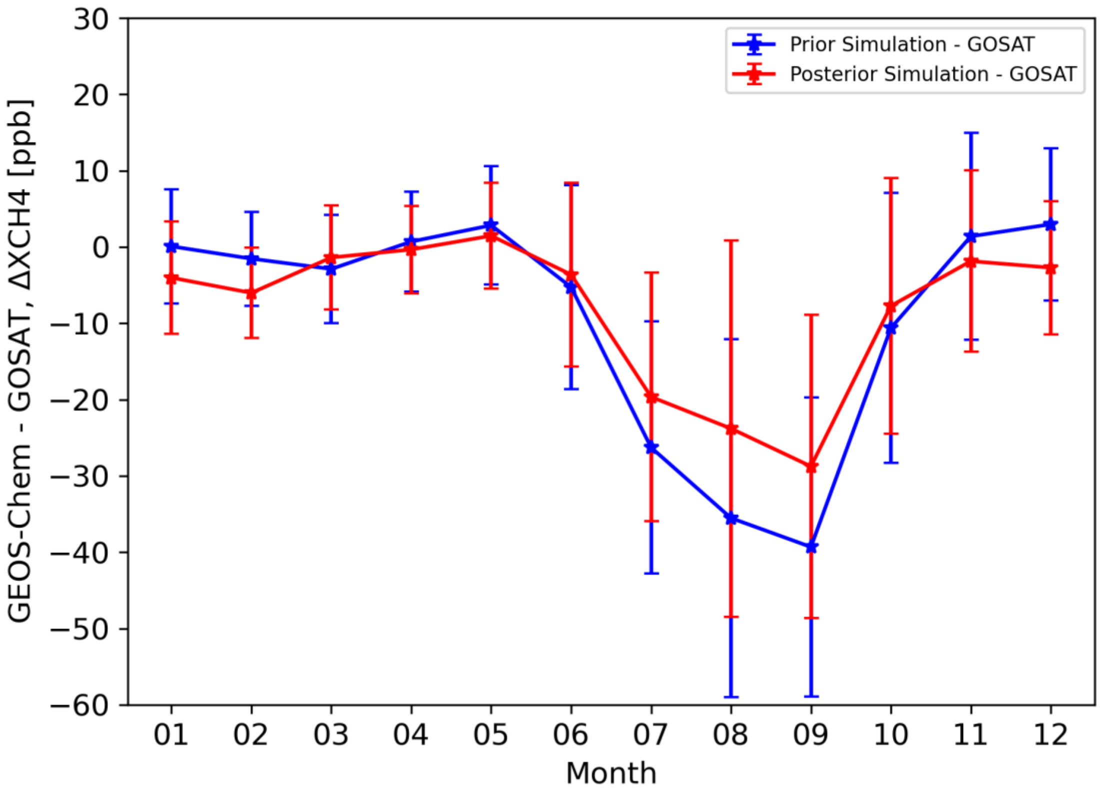

Figure R15.Monthly mean difference between GOSAT and GEOS-Chem prior (blue) and posterior (red) simulations over India. The error-bar represents one standard deviation of the monthly model–GOSAT differences.

Figure S8, large fluctuations exist between in-situ measurements and model simulations, with partial deviations exceeding 200 ppb. There needs in-depth analysis on the causes of such substantial discrepancies.

Author Response:

The Nainital surface-based station is in a complex mountainous environment, where large differences can arise when comparing point-based surface observations with relatively coarse-resolution transport simulations. The complex topography can further degrade the agreement, with the observed deviations likely reflecting local-scale effects that are not adequately represented in the model. A sentence has been added in line 413:

"The relatively large differences between the model simulations and surface observations at Nainital may partly reflect the complex mountainous terrain surrounding the station. The point measurements are influenced by local-scale processes and topographic effects that may not be fully resolved by the relatively coarse-resolution transport model, potentially contributing to the observed discrepancies."

Technical

Table 1 (Supplement): the seeps sensitivity entry, given as 0.1 with a range of 0.3 to 0.6, appears inconsistent, so please check it.

- Thank you for pointing this out. It should be 0.3 instead of 0.1. We have modified Table 1 accordingly.

Clarify in Sect. 3.1 the partition of the bias and RMSE improvement between boundary-condition optimization and interior emission adjustment.

- The sentence has been added at Line 370:

"Optimizing the boundary conditions alone reduces the mean bias from 2.1 ppb to 1.5 ppb and the RMSE from 14.3 ppb to 13.6 ppb, indicating that emission optimization makes a larger contribution to the overall improvement."

References:

Apituley, A.: Sentinel-5 precursor/TROPOMI Level 2 Product User Manual Methane, 2022.

Balasus, N., Jacob, D. J., Lorente, A., Maasakkers, J. D., Parker, R. J., Boesch, H., Chen, Z., Kelp, M. M., Nesser, H., and Varon, D. J.: A blended TROPOMI+GOSAT satellite data product for atmospheric methane using machine learning to correct retrieval biases, Atmos. Meas. Tech., 16, 3787–3807, https://doi.org/10.5194/amt-16-3787-2023, 2023.

Chen, Z., Jacob, D. J., Gautam, R., Omara, M., Stavins, R. N., Stowe, R. C., Nesser, H., Sulprizio, M. P., Lorente, A., Varon, D. J., Lu, X., Shen, L., Qu, Z., Pendergrass, D. C., and Hancock, S.: Satellite quantification of methane emissions and oil–gas methane intensities from individual countries in the Middle East and North Africa: implications for climate action, Atmos. Chem. Phys., 23, 5945–5967, https://doi.org/10.5194/acp-23-5945-2023, 2023.

Dogniaux, M., Maasakkers, J. D., Girard, M., Jervis, D., McKeever, J., Schuit, B. J., Sharma, S., Lopez-Noreña, A., Varon, D. J., and Aben, I.: Global satellite survey reveals uncertainty in landfill methane emissions, Nature, 647, 397–402, https://doi.org/10.1038/s41586-025-09683-8, 2025.

Estrada, L. A., Varon, D. J., Sulprizio, M., Nesser, H., Chen, Z., Balasus, N., Hancock, S. E., He, M., East, J. D., Mooring, T. A., Oort Alonso, A., Maasakkers, J. D., Aben, I., Baray, S., Bowman, K. W., Worden, J. R., Cardoso-Saldaña, F. J., Reidy, E., and Jacob, D. J.: Integrated Methane Inversion (IMI) 2.0: an improved research and stakeholder tool for monitoring total methane emissions with high resolution worldwide using TROPOMI satellite observations, Geosci. Model Dev., 18, 3311–3330, https://doi.org/10.5194/gmd-18-3311-2025, 2025.

Gao, J., Guan, C., Zhang, B., and Li, K.: Decreasing methane emissions from China's coal mining with rebounded coal production, Environ. Res. Lett., 16, 124037, https://doi.org/10.1088/1748-9326/ac38d8, 2021.

Sadavarte, P., Pandey, S., Maasakkers, J. D., Lorente, A., Borsdorff, T., Denier Van Der Gon, H., Houweling, S., and Aben, I.: Methane Emissions from Superemitting Coal Mines in Australia Quantified Using TROPOMI Satellite Observations, Environ. Sci. Technol., 55, 16573–16580, https://doi.org/10.1021/acs.est.1c03976, 2021.

Sadavarte, P., Pandey, S., Maasakkers, J. D., Van Der Gon, H. D., Houweling, S., and Aben, I.: A high-resolution gridded inventory of coal mine methane emissions for India and Australia, Elem. Sci. Anthr., 10, 00056, https://doi.org/10.1525/elementa.2021.00056, 2022.

Scarpelli, T. R., Jacob, D. J., Maasakkers, J. D., Sulprizio, M. P., Sheng, J.-X., Rose, K., Romeo, L., Worden, J. R., and Janssens-Maenhout, G.: A global gridded (0.1° × 0.1°) inventory of methane emissions from oil, gas, and coal exploitation based on national reports to the United Nations Framework Convention on Climate Change, Earth Syst. Sci. Data, 12, 563–575, https://doi.org/10.5194/essd-12-563-2020, 2020.

Singh, A. K. and Kumar, J.: Fugitive Methane Emissions from Indian Coal Mining and Handling Activities: Estimates, Mitigation and Opportunities for its Utilization to Generate Clean Energy, Energy Procedia, 90, 336–348, https://doi.org/10.1016/j.egypro.2016.11.201, 2016.